analytical chemistry

Article

Cite This: Anal. Chem. 2019, 91, 7744−7748

pubs.acs.org/ac

Bubble-Nucleation-Based Method for the Selective and Sensitive Electrochemical Detection of Surfactants

Ruchiranga Ranaweera,[†] Carina Ghafari,[‡] and Long Luo*[,†]

[†]Department of Chemistry, Wayne State University, Detroit, Michigan 48202, United States

[‡]Chemistry Department, Kalamazoo College, Kalamazoo, Michigan 49006, United States

Supporting Information

ABSTRACT: We present the first bubble-nucleation-based electrochemical method for the selective and sensitive detection of surfactants. Our method takes advantage of the high surface activity of surfactant analyte to affect the electrochemical bubble nucleation and then transduces the change in nucleation condition to electrochemical signal for determining the surfactant concentration. Using this method, we demonstrate the quantitation of perfluorinated surfactants in water, a group of emerging environmental contaminants, with a remarkable limit of detection (LOD) down to 30 μg/L and a linear dynamic range of over 3 orders of magnitude. With the addition of a preconcentration step, we have achieved the LOD: 70 ng/L, the health advisory for perfluorooctanesulfonate (PFOS) and perfluorooctanoic acid (PFOA) in drinking water established by the U.S. Environmental Protection Agency. The experimental results are in quantitative agreement with our theoretical model derived from classical nucleation theory. Our method also exhibits an exceptional specificity for the surfactant analytes even in the presence of 1000-fold excess of nonsurfactant interference. This method has the potential to be further developed into a universal electrochemical detector for surfactant analysis because of its simplicity and the surface-activity-based detection mechanism.

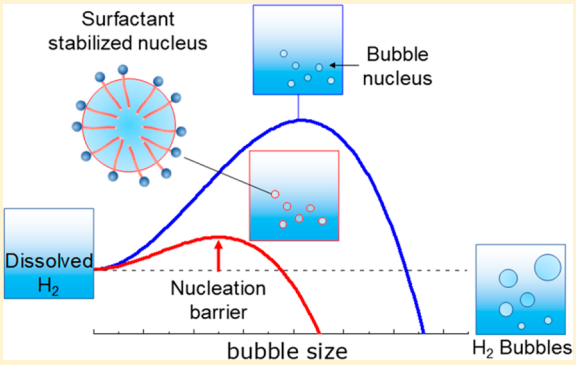

Surfactants are widely used as dispersants, emulsifiers, detergents, fabric softeners, and wetting agents in many household items and industrial products and processes.[1] Because of the environmental impact and toxicity of various surfactants, current legislation requires that the amount of surfactants released into the sewer system is minimized and that the concentrations in rivers and lakes are maintained at low levels.[2] For example, perfluorinated surfactants (PS) has been widely used in coating and surfactant applications since the 1950s (e.g., nonstick coating and fire-fighting foam) because of the chemical and thermal stability of a perfluoroalkyl moiety and its distinctive hydrophobic and lipophobic nature.[3,4] As a result of the extensive use of PS and their emission, a broad range of these compounds have been detected in the environment, wildlife, and humans. Recent biomedical studies have revealed the positive associations between PS exposure and disease parameters in the general population.[5] As a result, the U.S. Environmental Protection Agency identified addressing the problem of fluorinated substances as one of the national priorities in 2018.[6] Many well-known methodologies for surfactant determination require either expensive and complicated instruments (for example, liquid and gas chromatographs) or the use of relatively large amounts of organic solvents (such as chloroform in the spectroscopic "methylene blue" method),[7] making them unsuitable for in situ detection applications.[8] Therefore, there is a critical need to develop new and improved methods for surfactant detection.

The formation and evolution of vapor and gas bubbles in a liquid body is a phenomenon of vast fundamental and applicative interest, for example, in commercial electrolytic processes,[9,10] in cavitation,[11−13] in biomedical applications,[14−16] and in functional material fabrication.[17−20] Here, we present a new application of gas bubbles for surfactant detection. Our method is based on the interactions between gas nuclei and surfactant molecules during electrochemical gas bubble nucleation. According to classical nucleation theory (CNT),[21] nucleation of a gas bubble requires a supersaturation of dissolved gas because of the energy barrier of establishing a new gas−liquid interface (Scheme 1). In the presence of surfactant molecules, gas nuclei can be stabilized because of the reduced surface tension of the gas−liquid interface, leading to a decrease of the supersaturation level required for bubble nucleation. In our method, we take advantage of the high surface activity of surfactant analyte to affect the bubble nucleation, and transduce the change in the supersaturation level required for bubble nucleation to electrochemical signal for highly sensitive and specific detection of surfactant analytes.

Received: February 27, 2019
Accepted: April 26, 2019
Published: April 26, 2019

DOI: 10.1021/acs.analchem.9b01060
Anal. Chem. 2019, 91, 7744−7748

Scheme 1. Bubble-Nucleation-Based Electrochemical Method for Surfactant Detection[a]

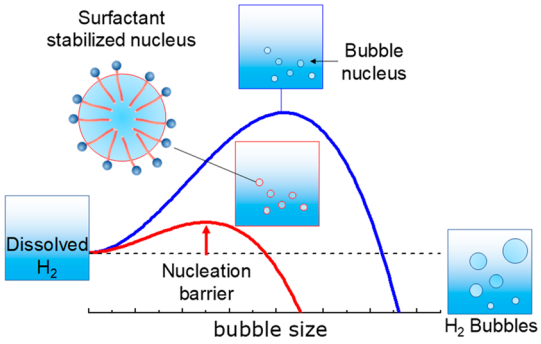

[a]Because of the high surface activity of surfactant molecules, they stabilize H_2 bubble nuclei, leading to a reduced nucleation barrier.

EXPERIMENTAL SECTION

Chemicals and Materials. Perchloric acid ($HClO_4$, 70%), sodium perchlorate ($NaClO_4$, 98%), tridecafluorohexane-1-sulfonic acid, nonafluorobutane-1-sulfonic acid, perfluorooctanoic acid, perfluoroheptanoic acid, undecafluorohexanoic acid, heptafluorobutyric acid, poly(ethylene glycol) (400 g/mol), TWEEN 20, lysozyme from chicken egg white, and humic acid were purchased from Sigma-Aldrich. Potassium perfluorooctanesulfonate was purchased from Matrix Scientific. Perfluoroheptanesulfonic acid was purchased from Synquest Laboratories. Glass capillary (outside diameter/inside diameter, 1.65/1.10 mm, soft temperature, 712 °C) was received from Dagan Corporation. Platinum (Pt wire, 25 μm diameter, 99.95%) wires were purchased from Surepure Chemetals. Silver conductive epoxy was purchased from MG Chemicals. A Visiprep SPE Vacuum manifold (Supelco Inc., Bellefonte, PA, USA) was used for solid-phase extraction. BondElut LMS polymer 500 mg SPE cartridges were purchased from Agilent. Surface tension measurements were conducted using the pendant drop method on a Kruss DSA100 goniometer. All aqueous solutions were prepared from deionized (DI) water (PURELAB, 18.2 MΩ cm, total organic carbon < 3 ppb).

Electrochemical Measurements. All experiments were carried out using a CHI 760E potentiostat and inside a grounded Faraday cage. An Ag/AgCl electrode in a saturated KCl solution was used as the counter/reference electrode during the measurements with nanoelectrodes. A mixture of 0.10 M $NaClO_4$ and 1.0 M $HClO_4$ was used as the supporting electrolyte for all the experiments. A serial dilution of perfluorinated surfactants was made in 1.0 M $HClO_4$/0.10 M $NaClO_4$ solution. Cyclic voltammograms of nanoelectrodes were run to obtain the peak current for each compound with different concentrations. The scan rate was fixed at 100 mV/s.

Nanoelectrode Fabrication Method. Pt nanoelectrodes were fabricated according to a previously reported method with some modifications.[22] A 1.5 cm long Pt wire was attached to a tungsten rod using Ag conductive epoxy. The end of the Pt wire was electrochemically etched to make a sharp point in 15 wt % $CaCl_2$ solution. With use of a function generator, 110 Hz sinusoidal wave with an amplitude of 4.3 V was applied to the Pt wire for 60 s. Sharpened wire was washed with deionized water and was then inserted into a glass capillary and thermally sealed using a H_2−O_2 flame. The sealing was inspected against possible gas bubbles using an optical microscope during the sealing process. Then the sealed tip was polished successively using silicon carbide polishing sandpapers (Buehler with grid size 600 and 1200) until a Pt nanodisk was exposed, which was monitored by an electronic feedback circuit. The radii of nanodisk electrodes, r, were determined by the diffusion-limited current for proton reduction (i_{lim}) in 0.10 M $HClO_4$ solution containing 0.10 M $NaClO_4$. The migration effects are suppressed by adding 0.10 M $NaClO_4$ as the supporting electrolyte. The radii were calculated using the following equation: $i_{lim} = 4nFDCr$, where D is the diffusion coefficient of H^+ and C is the concentration of $HClO_4$, respectively. A literature value of $D = 7.8 \times 10^{-5}$ cm^2/s was used.[23] The radii estimated using this method are within 10% difference from the ones determined from the conventional ferrocene oxidation method.

Preconcentration Method. Sample preconcentration was carried out using solid-phase extraction following U.S. EPA Method 537.[4] Briefly, the solid-phase extraction cartridge cleanup and conditioning was done with 15 mL of methanol followed by 18 mL of DI water. One liter of sample was passed through the cartridge at an approximate rate of 10−15 mL/min with the help of a vacuum manifold. Then the analyte was eluted from the cartridge with 15 mL of methanol. The eluate was collected and completely dried under a gentle stream of N_2 in a heated water bath (60−65 °C). Finally, 1.0 mL of 1.0 M $HClO_4$/0.10 M $NaClO_4$ solution was added to solvate the dried sample for electrochemical bubble-nucleation experiments.

RESULTS AND DISCUSSION

To electrochemically probe the bubble-nucleation condition, we adopted a nanoelectrode-based approach developed by Luo and White.[24] In this approach, a sub-50-nm Pt nanoelectrode is used to perform hydrogen evolution reaction (HER) in acid solutions. As the nanoelectrode potential is scanned negatively, the HER current increases exponentially until it reaches a peak value (i_{peak}). Past i_{peak}, the HER current immediately drops to a minimal value, which corresponds to the nucleation and formation of a gas bubble at the nanoelectrode, blocking the electrode surface.[24−26] The supersaturation level of dissolved H_2 gas required for H_2 bubble nucleation is proportional to the i_{peak} value.[24]

We chose perfluorooctanesulfonate (PFOS) and perfluorooctanoate (PFOA) as the model analytes because they have been found at the highest frequency and concentration in the environment and humans among all PS. The PS pattern in global river waters reveals that PFOS and PFOA account for ∼60% of the total mass concentration of PS.[27−33] This percentage is up to >80% in biological samples such as human milk and serum because of the bioaccumulation of PFOA and PFOS.[34] Figure 1a shows the cyclic voltammograms of an 11 nm radius Pt nanoelectrode in PFOS-containing $HClO_4$ solutions. All voltammograms at various concentrations of PFOS (C_{PFOS}) exhibited a cathodic peak at ca. −0.3 V, corresponding to the H_2 bubble nucleation and formation at the nanoelectrode surface. The C_{PFOS} was varied from 10^{-4} to 10^{-1} g/L. As C_{PFOS} increases, i_{peak} decreases. When i_{peak} is plotted against log(C_{PFOS}), there is a good linear relationship between them ($R^2 = 0.92$) with a slope of −0.82 nA/dec (Figure 1b). The LOD based on 3 times the standard deviation of the blank (i.e., in the absence of PFOS) is calculated to be 80 μg/L. The reduced i_{peak} in response to the increasing PFOS concentration is consistent with the detection mechanism that PFOS stabilizes bubble nuclei and, therefore, lowers the supersaturation requirement for bubble nucleation.

The same linear response has also been observed for PFOA, the other dominant PS contaminant, and the carboxylic acid

DOI: 10.1021/acs.analchem.9b01060
Anal. Chem. 2019, 91, 7744−7748

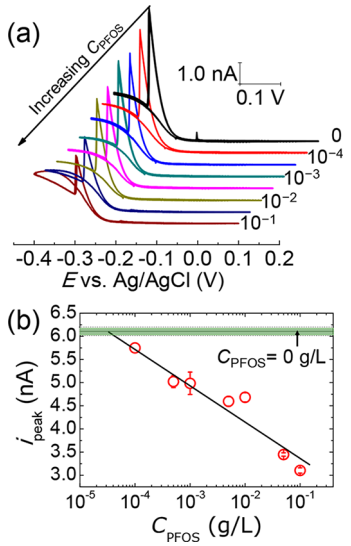

Figure 1. (a) Cyclic voltammograms for an 11 nm radius Pt nanoelectrode in 1.0 M $HClO_4$ containing 0.1 M $NaClO_4$ and various PFOS concentrations (g/L): 0, 10^{-4}, 5×10^{-4}, 10^{-3}, 5×10^{-3}, 10^{-2}, 5×10^{-2}, and 10^{-1}. Scan rate = 100 mV/s. (b) Plot of i_{peak} vs C_{PFOS}. Error bars are the standard deviations at each C_{PFOS} from at least three measurements. The best fit of the data points is plotted with $R^2 = 0.92$, which has a slope of −0.82 nA/dec. The horizontal black line shows the mean value of i_{peak} in the absence of PFOS and the corresponding standard deviation is highlighted in green. The LOD based on 3 times the standard deviation of the blank is calculated to be 80 μg/L.

counterpart of PFOS, in the same concentration range (Figure S1, Supporting Information). The obtained LOD for PFOA is 30 μg/L, which is slightly better than that for PFOS. It should be caused by the higher surface activity of PFOA than PFOS (their corresponding surface tension minima in water are 15.2 and 34.5 dyn/cm, respectively).[35] The LODs of our detection method for PFOA and PFOS are ∼2 orders of magnitude better than those of suppressed conductivity detection (∼2 mg/L)[36] and slightly worse than those of tandem mass spectrometry detection (∼0.5 μg/L),[4] the two most common detection methods for surfactant analysis used in high-performance liquid chromatography.

We further tested PS compounds with different fluoroalkyl chain lengths using our method. Figure 2 shows the plot of the

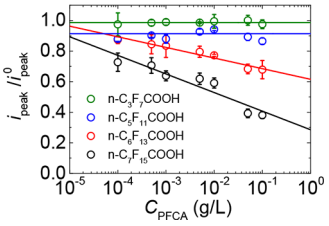

Figure 2. Plots of the normalized peak current (i_{peak}/i^0_{peak}) vs the concentration of perfluorinated carboxylic acids (C_{PFCA}) with different alkyl chain lengths. i^0_{peak} is the peak current at $C_{PFCA} = 0$.

peak current against the concentration of perfluorinated carboxylic acids (PFCA) with fluoroalkyl chain length, n = 3, 5, 6, and 7. The peak currents are normalized with respect to the peak current in the absence of PFCA to account for the nanoelectrode size effect as larger electrodes require larger currents to nucleate a bubble.[23,26,37] The corresponding unnormalized data are provided in Figure S2. As n decreases from 7 to 3, the slope is reduced from −0.12 dec^{-1} at n = 7 to −0.07 dec^{-1} at n = 6 and becomes close to 0 when n = 5 and 3. The trend of sensitivity change is consistent with the order of surface activity: n-C_7F_{15}COOH > n-C_6F_{13}COOH > n-C_5F_{11}COOH > n-C_3F_7COOH (Figure S3), further confirming our mechanism in Scheme 1. A similar trend has also been observed for perfluoroalkyl sulfonate compounds (Figure S4).

To quantitatively understand the detector response, we derived the expression of i_{peak} as a function of C_{PFOS}. According to CNT, the formation free energy of a gas bubble in solution, ΔG_{bubble}, is the sum of the energy cost of creating a new gas/liquid interface and the energy gain through the liberation of dissolved gas into the bubble volume, as expressed by eq 1.[38]

$$\Delta G_{bubble} = 4\pi\gamma r_{bubble}^{\ 2} + \frac{4\pi}{3}\Delta G_V r_{bubble}^{\ 3} \quad (1)$$

where γ is the surface tension of the gas/liquid interface and ΔG_V is the energy difference between the dissolved and gaseous state of the molecule in that volume. ΔG_{bubble} initially increases as a function of r_{bubble} before reaching a peak value, $E_{nuc} = \frac{16\pi\gamma^3}{3(\Delta G_V)^2}$, which is the nucleation energy barrier depicted in Scheme 1. Bubbles that overcome this energy barrier are energetically favored to continue to grow; otherwise, they are inclined to shrink and return to the dissolved form. Because bubbles of the critical size necessarily arise from the growth of subcritical nuclei, their formation relies upon relatively improbable fluctuations along the free energy barrier. The rate of critical nuclei formation or nucleation rate, J, is thus governed by the Arrhenius equation:

$$J = Z\exp\left(-\frac{E_{nuc}}{kT}\right) = Z\exp\left(-\frac{16\pi\gamma^3}{3\Delta G_V^{\ 2}kT}\right) \quad (2)$$

In the experiment, we scanned the potential of a nanoelectrode negatively at a constant scan rate (that is, a fixed duration time at each potential) to nucleate a H_2 gas bubble, and then we recorded the i_{peak}. Because the time required to nucleate a bubble defines the nucleation rate (J), when the duration time is fixed, we are setting a threshold value for J and seeking for the minimum current to reach this value. Hence, eq 2 can be rearranged and simplified to be

$$\Delta G_{V,nuc} = A\gamma^{3/2} \quad (3)$$

where A is a constant $\left(=\left(\frac{16\pi}{3kT\ln(Z/J)}\right)^{1/2}\right)$ and $\Delta G_{V,nuc}$ is the volume energy difference of the gas molecules when a bubble nucleates.

On the left side of eq 3, $\Delta G_{V,nuc}$ can be expressed as a function of i_{peak}.[39,40]

$$\Delta G_{V,nuc} = \frac{i_{peak}}{K_H 4nFD_{H_2}r} - P_{ambient} \quad (4)$$

where K_H is Henry's law constant for H_2 gas, D_{H_2} is the diffusion coefficient of H_2, n is the number of electrons transferred per H_2 (=2), F is Faraday's constant, r is the nanoelectrode radius, and $P_{ambient}$ is the ambient pressure.

On the right side of eq 3, γ is a nonlinear function of C_{PFOS} governed by the Gibbs equation.[41] We measured γ of the PFOS-containing solutions by the pendant drop method (Figure S5). The plot of γ versus $\log(C_{PFOS})$ in Figure 3a reveals an excellent linear relationship at the concentration range from 10^{-4} to 10 g/

DOI: 10.1021/acs.analchem.9b01060
Anal. Chem. 2019, 91, 7744−7748

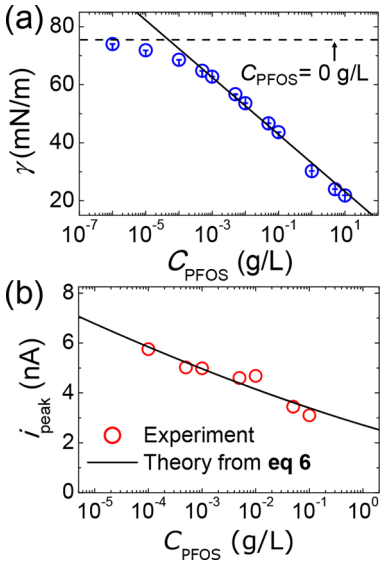

Figure 3. (a) Surface tension of PFOS-containing $HClO_4$ solutions measured by the pendant drop method. The best fit of the data points for $C_{PFOS} = 10^{-4}$ to 10 g/L is represented by the solid black line with $R^2 = 0.99$ and a slope of −9.8 mN/m·dec. (b) Comparison of experimental data and theoretical fit in the form of eq 6.

L. Outside this range, the data starts deviating from the linearity. Accordingly, γ can be numerically expressed by

$$\gamma = a \log(C_{PFOS}) + b \quad (5)$$

with $a = -9.8$ and $b = 33$ for $C_{PFOS} = 10^{-4}$ to 10 g/L. The linear function intercepts with the γ value of the blank ($C_{PFOS} = 0$) at $C_{PFOS} = \sim 50$ μg/L, which is consistent with the experimental LOD of ~80 μg/L for PFOS. Substituting eq 4 and eq 5 into eq 3, we obtain the following expression of i_{peak}.

$$i_{peak} = K_H 4nFD_{H_2} r[A(a \log(C_{PFOS}) + b)^{3/2} + P_{ambient}] \quad (6)$$

The experimental data agree very well with the theoretical fit in the form of eq 6 (Figure 3b), which again confirms our proposed bubble-nucleation-based detection mechanism. From the above derivation, we can conclude the nearly linear relationship between i_{peak} and $\log(C_{PFOS})$ originates from the linear dependence of the γ on $\log(C_{PFOS})$. Therefore, the sensitivity of this detection method is determined by the surface activity of analytes. Additionally, eq 6 also predicts that the electrode size (r) and properties of electrogenerated gas (D_{H_2}, K_H, and n) will contribute to the sensitivity of this method.

The native LOD of our detection method is around 30 and 80 μg/L for PFOA and PFOS, which are limited by the surface activity of these two compounds. These values are ~3 orders of magnitude higher than the desired LOD: 70 ng/L, which is the health advisory for PFOS and PFOA in drinking water established by the U.S. EPA.[6] This challenge can be overcome by adding a preconcentration step using solid-phase extraction which is currently used in the standard U.S. EPA method for PS analysis.[4] Figure 4 shows the LOD for PFOS was improved to ~40 ng/L after a 1000-fold preconcentration step using solid-phase extraction. The corresponding CVs are provided in Figure S6.

We further tested the specificity of this method for detecting surfactant analytes by adding an excess of nonsurfactant interference, poly(ethylene glycol) (PEG, 400 g/mol), which has a similar molecular weight as PFOS. Figure 5a shows the cyclic voltammograms of a Pt nanoelectrode in the presence of 1 mg/L PFOS and a 10-, 100-, and 1000-fold excess of PEG. The addition of PEG leads to a negative shift of the HER onset potential as compared to the PFOS-only sample, but the i_{peak} does not show any notable difference (Figure 5b). Apart from that, we have also tested different concentrations of humic acid and lysozyme. We observed no trend in the peak current compared to that of the blank (Figure S7). These results show the exceptional specificity of our method for surfactant analytes. However, we would like to point out that we did not observe the peak current change for a neutral surfactant, Tween-20 (Figure S7). The reason for this unusual behavior is currently under investigation.

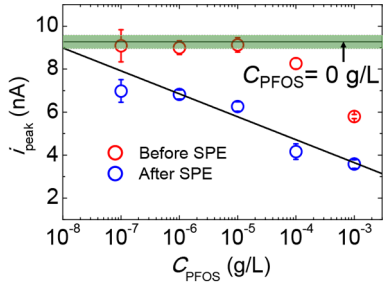

Figure 4. Plot of i_{peak} vs C_{PFOS} for PFOS samples before and after preconcentration using solid-phase extraction (SPE). The data after SPE is linearly fitted with $R^2 = 0.92$ and a slope of −1.1 nA/dec. The horizontal black line shows the mean value of i_{peak} in the absence of PFOS. The corresponding standard deviation is highlighted in green. The LOD based on 3 times the standard deviation of the blank is calculated to be 40 ng/L.

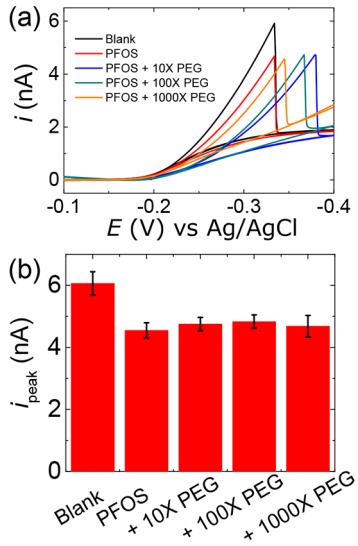

Figure 5. (a) Cyclic voltammograms and (b) the corresponding average i_{peak} for a 7 nm radius Pt nanoelectrode in 1.0 M $HClO_4$ containing 0.1 M $NaClO_4$, 1.0 mg/L PFOS, and a 10- to 1000-fold excess of poly(ethylene glycol) (PEG, 400 g/mol). Scan rate = 100 mV/s.

CONCLUSIONS

In conclusion, we have presented a bubble-nucleation-based electrochemical detection method for surfactant analysis for the

DOI: 10.1021/acs.analchem.9b01060
Anal. Chem. 2019, 91, 7744−7748

first time. This method has a high specificity for surfactant analytes, a broad linear dynamic range of over 3 orders of magnitude, and a remarkable LOD of ~30 μg/L (~2 orders of magnitude better than suppressed conductivity detection, a conventional detection method for surfactant analysis). With a preconcentration step, we have demonstrated the improvement of the LOD for PFOS to the target LOD. We have also established the theory for this new method. This method has the potential to be developed into a universal electrochemical detector for surfactant analysis.

■ ASSOCIATED CONTENT

Supporting Information

The Supporting Information is available free of charge on the ACS Publications website at DOI: 10.1021/acs.analchem.9b01060.

Plot of i_{peak} vs C_{PFOA}; plots of i_{peak} vs PS concentrations of different perfluoroalkylcarboxylic acids; photographs showing pendant drop shapes with different alkyl chain lengths; plots of i_{peak} vs PS concentrations of different perfluoroalkyl sulfonates; photographs showing pendant drop shapes with different PFOS concentrations; cyclic voltammograms of nanoelectrodes for PFOS samples with and without SPE preconcentration; plots of the normalized peak current (i_{peak}/i^0_{peak}) vs the concentration of humic acid, lysozyme, and Tween-20 (PDF)

■ AUTHOR INFORMATION

Corresponding Author

*E-mail: long.luo@wayne.edu.

ORCID

Long Luo: 0000-0001-5771-6892

Notes

The authors declare no competing financial interest.

■ ACKNOWLEDGMENTS

This work was supported by start-up funds, Ebbing Faculty Development Award, and University Research Grant from Wayne State University.

■ REFERENCES

(1) Kronberg, B.; Lindman, B. *Surfactants and polymers in aqueous solution*; John Wiley & Sons Ltd.: Chichester, 2003.

(2) Zoller, U. *Handbook of detergents, Part B: Environmental impact*; CRC Press: 2004; Vol. *121*.

(3) Kissa, E. *Fluorinated surfactants and repellents*; CRC Press, 2001; Vol. *97*.

(4) Shoemaker, J.; Grimmett, P.; Boutin, B. Method 537. Determination of Selected Perfluorinated Alkyl Acids in Drinking Water by Solid Phase Extraction and Liquid Chromatography/Tandem Mass Spectrometry (LC/MS/MS). https://cfpub.epa.gov/si/index.cfm (accessed Feb 26, 2019).

(5) Grandjean, P.; Clapp, R. *New Solut* **2015**, *25*, 147−163.

(6) U.S. Environmental Protection Agency *National Priorities: Per- and Polyfluoroalkyl Substances*. https://www.epa.gov/research-grants/national-priorities-and-polyfluoroalkyl-substances (accessed Feb 26, 2019).

(7) Clesceri, L. S.; Greenberg, A. E.; Eaton, A. D. *Standard Methods for the Examination of Water and Wastewater*, 20th ed.; American Public Health Association: 1999.

(8) Coll, C.; Martínez-Máñez, R.; Marcos, M. D.; Sancenón, F.; Soto, J. *Angew. Chem., Int. Ed.* **2007**, *46*, 1675−1678.

(9) Zhao, X.; Ranaweera, R.; Luo, L. *Chem. Commun.* **2019**, *55*, 1378−1381.

(10) Xu, W.; Lu, Z.; Sun, X.; Jiang, L.; Duan, X. *Acc. Chem. Res.* **2018**, *51*, 1590−1598.

(11) Chung, M.-F.; Chen, K.-J.; Liang, H.-F.; Liao, Z.-X.; Chia, W.-T.; Xia, Y.; Sung, H.-W. *Angew. Chem., Int. Ed.* **2012**, *51*, 10089−10093.

(12) Plesset, M. S.; Prosperetti, A. *Annu. Rev. Fluid Mech.* **1977**, *9*, 145−185.

(13) Blake, J. R.; Gibson, D. *Annu. Rev. Fluid Mech.* **1987**, *19*, 99−123.

(14) Shao, J.; Xuan, M.; Dai, L.; Si, T.; Li, J.; He, Q. *Angew. Chem., Int. Ed.* **2015**, *54*, 12782−12787.

(15) Zlitni, A.; Janzen, N.; Foster, F. S.; Valliant, J. F. *Angew. Chem., Int. Ed.* **2014**, *53*, 6459−6463.

(16) Chung, M.-F.; Liu, H.-Y.; Lin, K.-J.; Chia, W.-T.; Sung, H.-W. *Angew. Chem., Int. Ed.* **2015**, *54*, 9890−9893.

(17) Zhang, L.; Zhou, L.; Xu, N.; Ouyang, Z. *Angew. Chem., Int. Ed.* **2017**, *56*, 8191−8195.

(18) Pagano, J. J.; Bánsági, T., Jr; Steinbock, O. *Angew. Chem., Int. Ed.* **2008**, *47*, 9900−9903.

(19) Drenckhan, W. *Angew. Chem., Int. Ed.* **2009**, *48*, 5245−5247.

(20) Wang, Y.; Zheng, Y.; Xu, X.; Dubuisson, E.; Bao, Q.; Lu, J.; Loh, K. P. *ACS Nano* **2011**, *5*, 9927−9933.

(21) Blander, M.; Katz, J. L. *AIChE J.* **1975**, *21*, 833−848.

(22) Zhang, B.; Galusha, J.; Shiozawa, P. G.; Wang, G.; Bergren, A. J.; Jones, R. M.; White, R. J.; Ervin, E. N.; Cauley, C. C.; White, H. S. *Anal. Chem.* **2007**, *79*, 4778−4787.

(23) Chen, Q.; Ranaweera, R.; Luo, L. *J. Phys. Chem. C* **2018**, *122*, 15421−15426.

(24) Luo, L.; White, H. S. *Langmuir* **2013**, *29*, 11169−11175.

(25) Chen, Q.; Luo, L.; White, H. S. *Langmuir* **2015**, *31*, 4573−4581.

(26) Chen, Q.; Luo, L.; Faraji, H.; Feldberg, S. W.; White, H. S. *J. Phys. Chem. Lett.* **2014**, *5*, 3539−3544.

(27) Huset, C. A.; Chiaia, A. C.; Barofsky, D. F.; Jonkers, N.; Kohler, H.-P. E.; Ort, C.; Giger, W.; Field, J. A. *Environ. Sci. Technol.* **2008**, *42*, 6369−6377.

(28) Loos, R.; Gawlik, B. M.; Locoro, G.; Rimaviciute, E.; Contini, S.; Bidoglio, G. *Environ. Pollut.* **2009**, *157*, 561−568.

(29) McLachlan, M. S.; Holmström, K. E.; Reth, M.; Berger, U. *Environ. Sci. Technol.* **2007**, *41*, 7260−7265.

(30) Nakayama, S.; Strynar, M. J.; Helfant, L.; Egeghy, P.; Ye, X.; Lindstrom, A. B. *Environ. Sci. Technol.* **2007**, *41*, 5271−5276.

(31) Murakami, M.; Imamura, E.; Shinohara, H.; Kiri, K.; Muramatsu, Y.; Harada, A.; Takada, H. *Environ. Sci. Technol.* **2008**, *42*, 6566−6572.

(32) So, M. K.; Miyake, Y.; Yeung, W. Y.; Ho, Y. M.; Taniyasu, S.; Rostkowski, P.; Yamashita, N.; Zhou, B. S.; Shi, X. J.; Wang, J. X.; Giesy, J. P.; Yu, H.; Lam, P. K. S. *Chemosphere* **2007**, *68*, 2085−2095.

(33) Yeung, L. W.; Yamashita, N.; Taniyasu, S.; Lam, P. K.; Sinha, R. K.; Borole, D. V.; Kannan, K. *Chemosphere* **2009**, *76*, 55−62.

(34) Kärrman, A.; Ericson, I.; van Bavel, B.; Darnerud, P. O.; Aune, M.; Glynn, A.; Lignell, S.; Lindström, G. *Environ. Health Perspect.* **2007**, *115*, 226−230.

(35) Shinoda, K.; Hato, M.; Hayashi, T. *J. Phys. Chem.* **1972**, *76*, 909−914.

(36) Hori, H.; Hayakawa, E.; Yamashita, N.; Taniyasu, S.; Nakata, F.; Kobayashi, Y. *Chemosphere* **2004**, *57*, 273−282.

(37) Chen, Q.; Luo, L. *Langmuir* **2018**, *34*, 4554−4559.

(38) Talanquer, V.; Oxtoby, D. W. *J. Chem. Phys.* **1995**, *102*, 2156−2164.

(39) German, S. R.; Edwards, M. A.; Ren, H.; White, H. S. *J. Am. Chem. Soc.* **2018**, *140*, 4047−4053.

(40) German, S. R.; Edwards, M. A.; Chen, Q.; Liu, Y.; Luo, L.; White, H. S. *Faraday Discuss.* **2016**, *193*, 223−240.

(41) Menger, F. M.; Rizvi, S. A. A. *Langmuir* **2011**, *27*, 13975−13977.

DOI: 10.1021/acs.analchem.9b01060
Anal. Chem. 2019, 91, 7744−7748